AFRL-SR-AR-TR-05-

0045

REPORT DOCUMENTATION PAGE

1. REPORT DATE (DD-MM-YYYY)	2. REPORT TYPE	3. DATES COVERED (From - To)
	Final	1 April 2001 - 31 December 2003

4. TITLE AND SUBTITLE	5a. CONTRACT NUMBER
Computational Algorithms for High-Fidelity Multidisciplinary design of Complex Aerospace Systems	
	5b. GRANT NUMBER
	F49620-01-1-0291
	5c. PROGRAM ELEMENT NUMBER

6. AUTHOR(S)	5d. PROJECT NUMBER
Anthony Jameson	
Juan J. Alonso	5e. TASK NUMBER
	5f. WORK UNIT NUMBER

7. PERFORMING ORGANIZATION NAME(S) AND ADDRESS(ES)	8. PERFORMING ORGANIZATION REPORT NUMBER
Department of Aeronautics & Astronautics Stanford University Stanford, CA 94305	

9. SPONSORING/MONITORING AGENCY NAME(S) AND ADDRESS(ES)	10. SPONSOR/MONITOR'S ACRONYM(S)
Air Force Office of Scientific Research 4015 Wilson Blvd Mail Room 713 Arlington, VA 22203	AFOSR
	11. SPONSOR/MONITOR'S REPORT NUMBER(S)

12. DISTRIBUTION/AVAILABILITY STATEMENT

Distribution Statement A. Approved for public release; distribution is unlimited.

13. SUPPLEMENTARY NOTES

14. ABSTRACT

The major objectives stated in our proposal have been completed and achieved.

During the first year, with the help of S. Nadarajah, a number of different studies on the suitability of the continuous and discrete adjoint formulations for design using the viscous Reynolds-Averaged Navier-Stokes equations were carried out. Our conclusion is that the implementation of the continuous formulation is more straightforward and leaves more freedom on the choices of discretization of the adjoint equations. We found, however, that the discrete adjoint approach can be very helpful in resolving some of the mathematical ambiguities that are left in the continuous approach when creating imposing boundary conditions.

15. SUBJECT TERMS

16. SECURITY CLASSIFICATION OF:			17. LIMITATION OF ABSTRACT	18. NUMBER OF PAGES	19a. NAME OF RESPONSIBLE PERSON
a. REPORT	b. ABSTRACT	c. THIS PAGE			Anthony Jameson
U	U	U	UU		19b. TELEPHONE NUMBER (Include area code)

Standard Form 298 (Rev. 8/98)
Prescribed by ANSI Std. Z39.18

Computational Algorithms for High-Fidelity Multidisciplinary Design of Complex Aerospace Systems

AFOSR GRANT NO. AF F49620-01-1-0291

FINAL REPORT

Antony Jameson and Juan J. Alonso
Department of Aeronautics & Astronautics
Stanford University
Stanford, CA 94305

Objectives

The objective of our AFOSR-sponsored work under this grant has been to advance the tools that are required to make high-fidelity multidisciplinary design of aerospace systems feasible. During this grant, our approach was based on the use of gradient-based optimization coupled with system sensitivity information that is inexpensively obtained via adjoint methods. Our effort was divided into two main components: the primary effort was focused on the application of adjoint techniques to the problem of aerodynamic shape optimization. The second effort developed a framework to extend the adjoint approach to treat additional disciplines in the design problem (structures, stability & control, propulsion, etc.), although in this work it has focused on the problem of aero-structural design.

Status of Effort

The major objectives stated in our proposal have been completed and achieved.

- During the first year, with the help of S. Nadarajah, a number of different studies on the suitability of the continuous and discrete adjoint formulations for design using the viscous Reynolds-Averaged Navier-Stokes equations were carried out. Our conclusion is that the implementation of the continuous formulation is more straightforward and leaves more freedom on the choices of discretization of the adjoint equations. We found, however, that the discrete adjoint approach can be very helpful in resolving some of the mathematical ambiguities that are left in the continuous approach when creating imposing boundary conditions.

- We have completed a new formulation for the adjoint gradient formulae which only depends on the evaluation of a surface integral. This *reduced gradient approach* has been tested within the context of structured meshes, but promised to resolve one of the major issues in the implementation of adjoint methods on unstructured meshes. We hope to pursue this matter in future work.

- During all of our optimizations, we have been investigating the possibility of using smoothing and/or preconditioning of the gradients to improve the convergence and robustness of the search procedure. Various examples are presented in this report.

- We have started performing planform optimization studies using the adjoint method. In the past, all of our work had fixed the planform of the aircraft and had focused on changes to the airfoil sections

1

along the span (in order not to influence the other disciplines that may have dictated the exact shape of the planform. We are now in a position to obtain accurate gradients of the cost functions of interest to changes in the planform shape (sweep, area, taper, etc.) We intend to continue this work and to include structural modeling capabilities to ensure that aerodynamic changes in the planform are not detrimental to the overall performance of the vehicle.

- We have developed a theoretical framework for the optimization of multi-disciplinary systems that allows the coupling of multiple adjoint solutions to provide overall system sensitivities. This method is rather promising in its application to high-fidelity design.

- We have also demonstrated this theoretical framework within the context of detailed aero-structural design, where both the shape of the aircraft and the shape and material distribution of the underlying structure are simultaneously changed to obtain improvements in performance measures that combine both aerodynamic and structural observations.

In our opinion, the result of this work has significantly advanced our knowledge in the application of adjoint techniques to both aerodynamic shape optimization and multi-disciplinary, aero-structural design problems. The following sections summarize the key results of this work. Detailed references are provided that include many more details on the derivations and applications of our methods.

Accomplishments

This section mirrors the actual work described above (also in our Statement of Objectives). Each section focuses on one of the elements of our mathematical formulations and design work.

Continuous vs. Discrete Adjoint Method Studies

The objective of this study was to compare the continuous and discrete adjoint-based automatic aerodynamic optimization approaches. Our intention was to study the trade-offs between the complexity of the discretization of the adjoint equation for both the continuous and discrete approaches, the accuracy of the resulting estimates of the gradients, and their impact on the computational cost to approach an optimum solution. For details on the derivation and implementation of the continuous adjoint method, please refer to the cited bibliography. We will briefly present the complete formulation of the discrete adjoint equation and will then investigate their differences. The similarities between the continuous and discrete boundary conditions are also explored. The results demonstrate two-dimensional inverse pressure design as well as the accuracy of the sensitivity derivatives obtained from continuous and discrete adjoint-based equations when compared to finite-difference gradients. More details can be found in the publications in the bibliography.

The discrete adjoint equation is obtained by applying the control theory directly to the set of discrete field equations. The resulting equation depends on the type of scheme used to solve the flow equations. The following discussion uses a cell centered multigrid scheme with upwind biased blended first and third order fluxes as the artificial dissipation scheme. A full discretization of the equation would involve discretizing every term that is a function of the state vector

$$\delta I = \delta I_c + \sum_{i=2}^{nx} \sum_{j=2}^{ny} \psi_{i,j}^T \delta \left(R(w)_{i,j} + D(w)_{i,j} \right), \tag{1}$$

where δI_c is the discrete cost function, $R(w)$ is the field equation, and $D(w)$ is the artificial dissipation term.

Terms multiplied by the variation $\delta w_{i,j}$ of the discrete flow variables are collected and the following is the resulting discrete adjoint equation,

$$V\frac{\partial \psi_{i,j}}{\partial t} =$$

$$\left(\Delta y_{\eta_{i+\frac{1}{2}},j}\left[\frac{\partial f}{\partial w}\right]_{i,j}^{T} - \Delta x_{\eta_{i+\frac{1}{2}},j}\left[\frac{\partial g}{\partial w}\right]_{i,j}^{T}\right)\frac{\psi_{i+1,j}}{2}$$

$$-\left(\Delta y_{\eta_{i-\frac{1}{2}},j}\left[\frac{\partial f}{\partial w}\right]_{i,j}^{T} - \Delta x_{\eta_{i-\frac{1}{2}},j}\left[\frac{\partial g}{\partial w}\right]_{i,j}^{T}\right)\frac{\psi_{i-1,j}}{2}$$

$$+\left(\Delta x_{\xi_{i,j+\frac{1}{2}}}\left[\frac{\partial g}{\partial w}\right]_{i,j}^{T} - \Delta y_{\xi_{i,j+\frac{1}{2}}}\left[\frac{\partial f}{\partial w}\right]_{i,j}^{T}\right)\frac{\psi_{i,j+1}}{2}$$

$$-\left(\Delta x_{\xi_{i,j-\frac{1}{2}}}\left[\frac{\partial g}{\partial w}\right]_{i,j}^{T} - \Delta y_{\xi_{i,j-\frac{1}{2}}}\left[\frac{\partial f}{\partial w}\right]_{i,j}^{T}\right)\frac{\psi_{i,j-1}}{2}$$

$$-\left(\Delta y_{\eta_{i+\frac{1}{2}},j}\left[\frac{\partial f}{\partial w}\right]_{i,j}^{T} - \Delta x_{\eta_{i+\frac{1}{2}},j}\left[\frac{\partial g}{\partial w}\right]_{i,j}^{T}\right)\frac{\psi_{i,j}}{2}$$

$$+\left(\Delta y_{\eta_{i-\frac{1}{2}},j}\left[\frac{\partial f}{\partial w}\right]_{i,j}^{T} - \Delta x_{\eta_{i-\frac{1}{2}},j}\left[\frac{\partial g}{\partial w}\right]_{i,j}^{T}\right)\frac{\psi_{i,j}}{2}$$

$$-\left(\Delta x_{\xi_{i,j+\frac{1}{2}}}\left[\frac{\partial g}{\partial w}\right]_{i,j}^{T} - \Delta y_{\xi_{i,j+\frac{1}{2}}}\left[\frac{\partial f}{\partial w}\right]_{i,j}^{T}\right)\frac{\psi_{i,j}}{2}$$

$$+\left(\Delta x_{\xi_{i,j-\frac{1}{2}}}\left[\frac{\partial g}{\partial w}\right]_{i,j}^{T} - \Delta y_{\xi_{i,j-\frac{1}{2}}}\left[\frac{\partial f}{\partial w}\right]_{i,j}^{T}\right)\frac{\psi_{i,j}}{2}$$

$$+\delta d_{i+\frac{1}{2},j} - \delta d_{i-\frac{1}{2},j} + \delta d_{i,j+\frac{1}{2}} - \delta d_{i,j-\frac{1}{2}},$$

$$(2)$$

where

$$\delta d_{i+\frac{1}{2},j} = \epsilon_{i+\frac{1}{2},j}^{2}(\psi_{i+1,j} - \psi_{i,j}) - \epsilon_{i+\frac{3}{2},j}^{4}\psi_{i+2,j}$$
$$+3\epsilon_{i+\frac{1}{2},j}^{4}(\psi_{i+1,j} - \psi_{i,j}) + \epsilon_{i-\frac{3}{2},j}^{4}\psi_{i-1,j}$$

$$(3)$$

is the discrete adjoint artificial dissipation term and V is the cell area. The dissipation coefficients ϵ^2 and ϵ^4 are functions of the flow variables, but to reduce complexity they are treated as constants.

In the case of an inverse design, δI_c is the discrete form of the square of the pressure integral around the airfoil surface. In contrast to the continuous adjoint, where the boundary condition appears as an update to the costate variables in the cell below the wall, the discrete boundary condition appears as a source term in the adjoint fluxes. At cell $i, 2$ the adjoint equation is as follows,

$$V\frac{\partial \psi_{i,2}}{\partial t} =$$
$$\frac{1}{2}\left[-A_{i-\frac{1}{2},2}^{T}(\psi_{i,2} - \psi_{i-1,2}) - A_{i+\frac{1}{2},2}^{T}(\psi_{i+1,2} - \psi_{i,2})\right]$$
$$+\frac{1}{2}\left[-B_{i,\frac{5}{2}}^{T}(\psi_{i,3} - \psi_{i,2})\right] + \Phi,$$

$$(4)$$

where V is the cell area, Φ is the source term for inverse design,

$$\Phi = \left(-\Delta y_{\xi}\psi_{2_{i,2}} + \Delta x_{\xi}\psi_{3_{i,2}} - (p - p_T)\Delta s_i\right)\delta p_{i,2},$$

and

$$A_{i+\frac{1}{2},2}^{T} = \Delta y_{\eta_{i+\frac{1}{2}},2}\left[\frac{\partial f}{\partial w}\right]_{i,2}^{T} - \Delta x_{\eta_{i+\frac{1}{2}},2}\left[\frac{\partial g}{\partial w}\right]_{i,2}^{T}.$$

All the terms in equation (4) except for the source term are scaled by the square of Δx. Therefore, as the mesh width is reduced, the terms within parenthesis in the source term divided by Δs_i must approach zero as

Grid Size	Cont.	Disc.	Cont-Disc
96 x 16	$3.106e-3$	$2.397e-3$	$9.585e-4$
192 x 32	$1.730e-3$	$1.724e-3$	$2.130e-4$
256 x 64	$1.424e-3$	$1.419e-3$	$4.749e-5$

Table 1: L_2 norm of the Difference Between Adjoint and Finite Difference Gradient

the solution reaches a steady state. One then recovers the continuous adjoint boundary condition described in earlier works.

If a first order artificial dissipation equation is used, then equation (3) would reduce to the term associated with ϵ^2. In such a case, the discrete adjoint equations are completely independent of the costate variables in the cells below the wall. However, if we use the blended first and third order dissipation, then these values are required. In practice, a simple zeroth order extrapolation across the wall produces good results.

Replacing the inverse design boundary condition in equation (4) by the discrete form of the cost function results in a discrete adjoint equation for drag minimization.

As an example of the results in the study, an inverse design test case is briefly shown here. The target pressure is first obtained using the FLO83 flow solver for the NACA 64A410 airfoil at a flight condition of $M = 0.74$ and a lift coefficient of $C_l = 0.63$ on a 192 x 32 C-grid. At such a condition the NACA 64A410 produces a strong shock on the upper surface of the airfoil, thus making it an ideal test case for the adjoint versus finite difference comparison.

The gradient for the continuous and discrete adjoint is obtained by perturbing each point on the airfoil. We apply an implicit smoothing technique to the gradient, before it is used to obtain a direction of descent for each point on the surface of the airfoil.

Figures (1), (2), and (3) exhibit the values of the gradients obtained from the adjoint methods and finite difference for various grid sizes. The circles denote values that we obtain by using the finite difference method. The square represents the discrete adjoint gradient. The asterisk represents the continuous adjoint gradient. The gradient is obtained with respect to variations in Hicks-Henne sine "bump" functions placed along the upper and lower surface of the airfoil. The figures only illustrate the values obtained from the upper surface starting from the leading edge on the left and ending at the trailing edge on the right.

Figure (4) presents the effect of the partial discretization of the flow solver to obtain the discrete adjoint equation. Here we obtain the finite difference gradients in the figure without freezing the dissipative coefficients. A small discrepancy exists in regions closer to the leading edge and around the shock.

Table 1 contains values of the L_2 norm of the difference between the adjoint and finite difference gradients. The table illustrates three important facts: the difference between the continuous adjoint and finite difference gradient is slightly greater than that between the discrete adjoint and finite difference gradient; the norm decreases as the mesh size is increased; and the difference between continuous and discrete adjoint gradients decreases as the mesh size is reduced. The second column depicts the difference between the continuous adjoint and finite difference gradient. The third column depicts the difference between the discrete adjoint and finite difference gradients. The last column depicts the difference between the discrete adjoint and continuous adjoint. As the mesh size increases the norms decrease as expected. Since we derive the discrete adjoint by taking a variation of the discrete flow equations, we expect it to be consistent with the finite difference gradients and thus to be closer than the continuous adjoint to the finite difference gradient. This is confirmed by numerical results, but the difference is very small. As the mesh size increases, the difference between the continuous and discrete gradients should decrease, and this is reflected in the last column of table 1.

In conclusion,

1. The continuous boundary condition appears as an update to the costate values below the wall for a cell-centered scheme, and the discrete boundary condition appears as a source term in the cell above the wall. As the mesh width is reduced, one recovers the continuous adjoint boundary condition from the discrete adjoint boundary condition.

2. Discrete adjoint gradients have better agreement than continuous adjoint gradients with finite difference gradients as expected, but the difference is generally small.
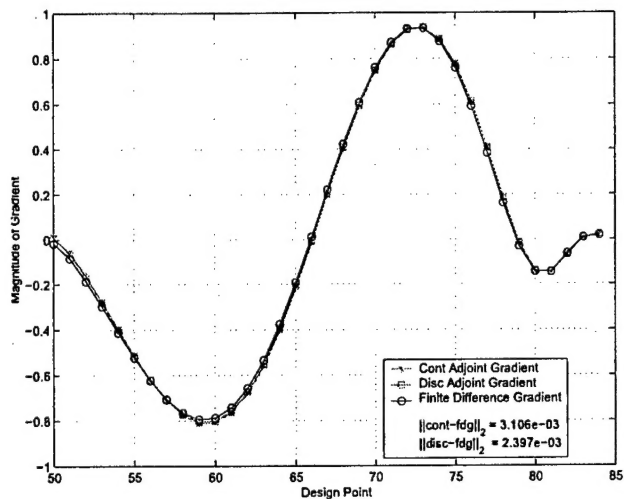
Figure 1: Adjoint Versus Finite Difference Gradients for Inverse Design of Korn to NACA 64A410 at Fixed C_l.
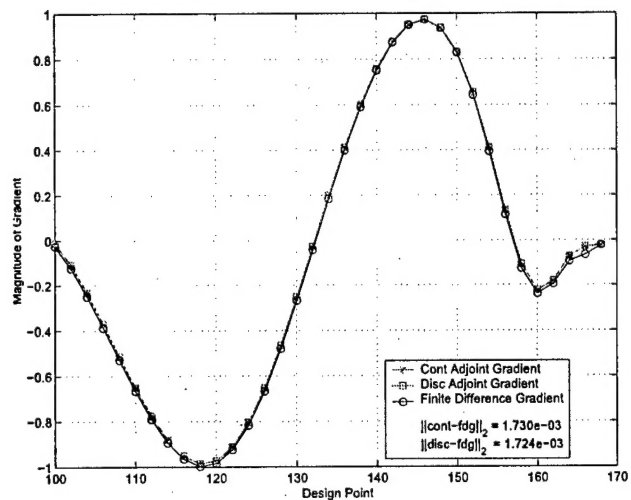Coarse Grid - 96 x 16, $M = 0.74$, $C_l = 0.63$

Figure 2: Adjoint Versus Finite Difference Gradients for Inverse Design of Korn to NACA 64A410 at Fixed C_l.
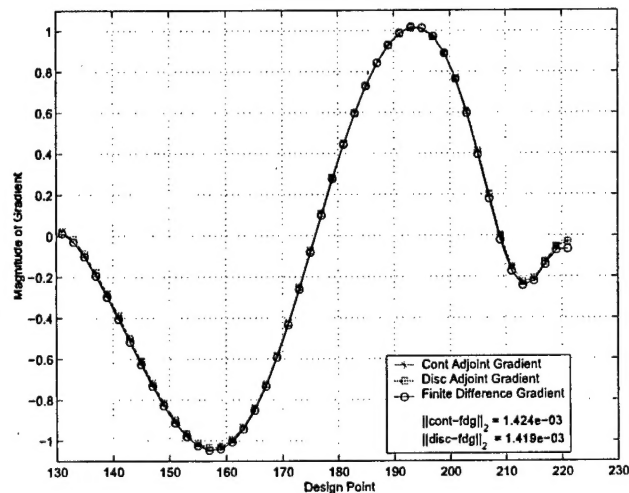Medium Grid - 192 x 32, $M = 0.74$, $C_l = 0.63$

Figure 3: Adjoint Versus Finite Difference Gradients for Inverse Design of Korn to NACA 64A410 at Fixed C_l.
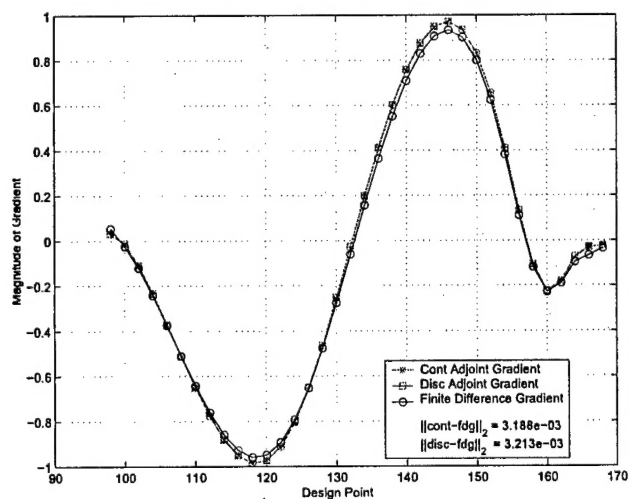Fine Grid - 256 x 64, $M = 0.74$, $C_l = 0.63$

Figure 4: Adjoint Versus Finite Difference Gradients for Inverse Design of Korn to NACA 64A410 at Fixed C_l. Dissipative Coefficients Not Frozen
Medium Grid - 192 x 32, $M = 0.74$, $C_l = 0.63$

5

3. As the mesh size increases, both the continuous adjoint gradient and the discrete adjoint gradient approach the finite difference gradient.

4. The difference between the continuous and discrete gradient reduces as the mesh size increases.

5. The cost of deriving the discrete adjoint is greater.

6. With our search procedure as outlined, the overall convergence of the objective function is not significantly affected when the discrete adjoint gradient is used instead of the continuous adjoint gradient. Consequently, we find no particular benefit in using the discrete adjoint method, which requires greater computational cost. However, we believe it beneficial to use the discrete adjoint equation as a guide for the discretization of the continuous adjoint equation.

Studies of Field Integral Elimination in Gradient Computations

A new continuous adjoint method for Aerodynamic Shape Optimization (ASO) using the Euler and Navier-Stokes equations has been developed. Using this new method large savings in the computation of the gradients of aerodynamic cost functions can be achieved by reducing the volume integral part of the adjoint gradient formula to a surface integral over the configuration of interest. The new method offers significant savings for three-dimensional ASO problems on general unstructured and overset meshes. In order to validate the concept, the new adjoint gradient equations were implemented and tested for drag minimization problems of a single-element airfoil and a three-dimensional wing-fuselage configuration. The accuracy of the resulting derivative information for the two-dimensional problem was investigated by direct comparison with finite-difference gradients and the original adjoint gradients which include the volume integral.

The Reduced Gradient Formulation

Using the adjoint formulation that has been used in our previous work, consider the case of a mesh variation with a fixed boundary. Then,

$$\delta I = 0,$$

where I is the cost function of interest. However, there is a variation in the transformed flux,

$$\delta F_i = C_i \delta w + \delta S_{ij} f_j.$$

Here the true solution is unchanged, so the variation δw is due to the mesh movement δx at fixed boundary configuration. Therefore

$$\delta w = \nabla w \cdot \delta x = \frac{\partial w}{\partial x_j} \delta x_j \, (= \delta w^*)$$

and since

$$\frac{\partial}{\partial \xi_i} \delta F_i = 0.$$

it follows that

$$\int_{\mathcal{D}} \phi^T \frac{\partial}{\partial \xi_i} \left(\delta S_{ij} f_j \right) d\mathcal{D} = -\int_{\mathcal{D}} \phi^T C_i \delta w^* d\mathcal{D}. \tag{5}$$

A similar relationship has been derived in the general case with boundary movement and the complete derivation will be presented in an upcoming conference paper. Now

$$
\begin{aligned}
\int_{\mathcal{D}} \phi^T \delta R d\mathcal{D} &= \int_{\mathcal{D}} \phi^T \frac{\partial}{\partial \xi_i} C_i \left(\delta w - \delta w^* \right) d\mathcal{D} \\
&= \int_{\mathcal{B}} \phi^T C_i \left(\delta w - \delta w^* \right) d\mathcal{B} \\
&\quad - \int_{\mathcal{D}} \frac{\partial \phi^T}{\partial \xi_i} C_i \left(\delta w - \delta w^* \right) d\mathcal{D}.
\end{aligned}
\tag{6}
$$

Here on wall boundary

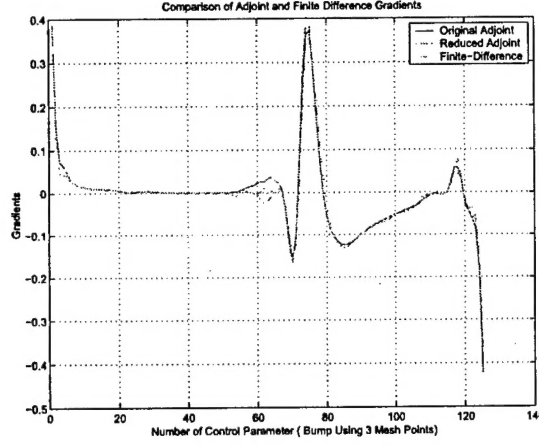$$C_2 \delta w = \delta F_2 - \delta S_{2j} f_j. \tag{7}$$

6

Figure 5: Euler Drag Minimization for RAE2822: Comparison of Original Adjoint, Reduced Adjoint and Finite-Difference Gradients Using 3 Mesh-Point Bump as Design Variable.

Thus, by choosing ϕ satisfying the adjoint equation and the adjoint boundary condition, we have finally the reduced gradient formulation that

$$\delta I = + \int_{\mathcal{B}_W} \psi^T \left(\delta S_{2j} f_j + C_2 \delta w^* \right) d\xi_1 d\xi_3$$
$$- \int\int_{\mathcal{B}_W} (\delta S_{21} \psi_2 + \delta S_{22} \psi_3 + S_{23} \psi_4)\, p \, d\xi_1 d\xi_3. \tag{8}$$

Gradient comparison for two-dimensional design

Computations were performed for an RAE 2822 airfoil at a fixed coefficient of lift, $C_l = 0.6$, and $M_\infty = 0.75$, using a C-mesh of size 192×32 for both the flow and adjoint solutions. Every mesh point on the airfoil was used as a design variable. In this case, a comparison with finite-difference gradients was not made, since accurate finite difference gradients cannot be calculated with the shape discontinuity caused by movement of a single mesh point. The gradients obtained using both the original and new adjoint formulas agree well in general. We believe that the new formulas may be sensitive to details of their discretization in regions of high curvature. A comparison with finite-difference gradients was also tried using local bump functions. In order to avoid geometric discontinuities, bumps were generated such that, while the same movement of each mesh point in turn was made as before, one-fourth of the movement was distributed to its two neighboring points, corresponding to local B-splines. Figure 5 shows a comparison between the gradients obtained using the three techniques. All three gradients agree quite well, although there is still a discrepancy near the leading edge.

Planform Design Studies

Cost Function for Planform Design

In order to design a high performance transonic wing, which will lead to a desired pressure distribution, and still maintain a realistic shape, the natural choice is to set

$$I = \alpha_1 C_D + \alpha_2 \frac{1}{2} \int_B (p - p_d)^2 dS + \alpha_3 C_W \tag{9}$$

with

$$C_W = \frac{\mathcal{W}_{wing}}{q_\infty S_{ref}} \tag{10}$$

7

where

C_D = drag coefficient,

C_W = normalized wing structure weight,

p = current surface pressure,

p_d = desired pressure,

q_∞ = dynamic pressure,

S_{ref} = reference area,

$\mathcal{W}_{wing}$ = wing structure weight, and

$\alpha_1, \alpha_2, \alpha_3$ = weighting constants.

A practical way to estimate $\mathcal{W}_{wing}$ is to use the so-called Statistical Group Weights Method, which applies statistical equations based on sophisticated regression analysis. For a cargo/transport wing weight, one can use

$$\mathcal{W}_{weight} = 0.0051(W_{dg}N_z)^{0.557}S_w^{0.649}A^{0.5}$$
$$(t/c)_{root}^{-0.4}(1+\lambda)^{0.1}cos(\Lambda)^{-1.0}S_{csw}^{0.1} \tag{11}$$

where

A = aspect ratio,

N_z = ultimate load factor; = 1.5 x limit load factor,

S_{csw} = control surface area (wing-mounted),

S_w = trapezoidal wing area,

t/c = thickness to chord ratio,

W_{dg} = flight design gross weight,

Λ = wing sweep, and

λ = taper ratio at 25 % MAC.

In addition, if the wing of interest is modeled by five planform variables such as root chord (c_1), mid-span chord (c_2), tip chord (c_3), span (b), and sweepback(Λ), as shown in Figure 6, it can be seen from the wing weight formula (11) that the weight is estimated to vary inversely with $cos(\Lambda)$, where Λ is the wing sweep.
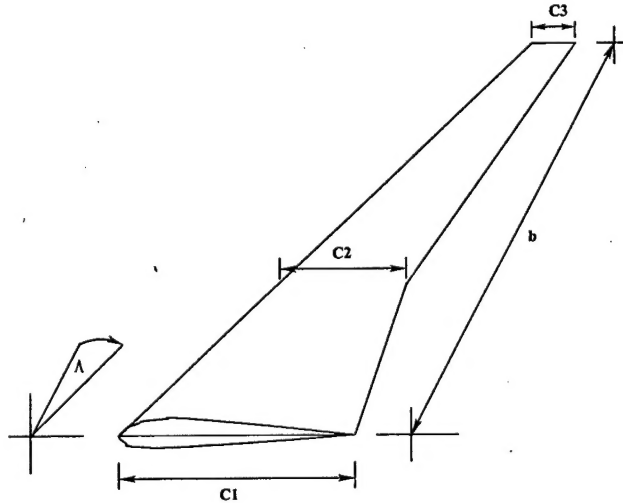

Figure 6: Modeled wing governed by five planform variables; root chord (c_1), mid-span chord (c_2), tip chord (c_3), span (b), and sweepback(Λ).

Here if the sweepback is allowed to vary and α_3 is chosen to be sufficiently large in the cost function (9), we should expect the optimization to decrease the sweepback angle at the cost of an increase in shock drag.

A change of span affects the wing weight of the wing weight formula (11) through changes of the trapezoidal wing area (S_w), the aspect ratio (A), and the wing-mounted area (S_{csw}). From the wing weight formula (11), an increase of span will cause S_w, A, and S_{csw} to increase, resulting in an increase of wing weight. Since induced drag varies inversely with the square of span, if the span is allowed to vary and α_3 is chosen to be sufficiently large, it is expected the optimizer to reduce the span at the cost of an increase in drag.

Variations of c_1, c_2, and c_3 affect the wing weight of the wing weight formula (11) via variations of aspect ratio (A), wing-mounted wing area (S_{csw}), trapezoidal wing area (S_w), and thickness to chord ratio (t/c). The effect of an individual chord change on the wing weight is plotted in Figure 7. Figure 7 shows that the wing weight of the Statistical Group Weights Method is a linear function of chord length. And because the slope varies along the span location, the change of chord at different span location will affect the wing weight differently. With the same change in chord length, the decrease of the mid-span chord (c_2) tends to give more weight reduction than the others.
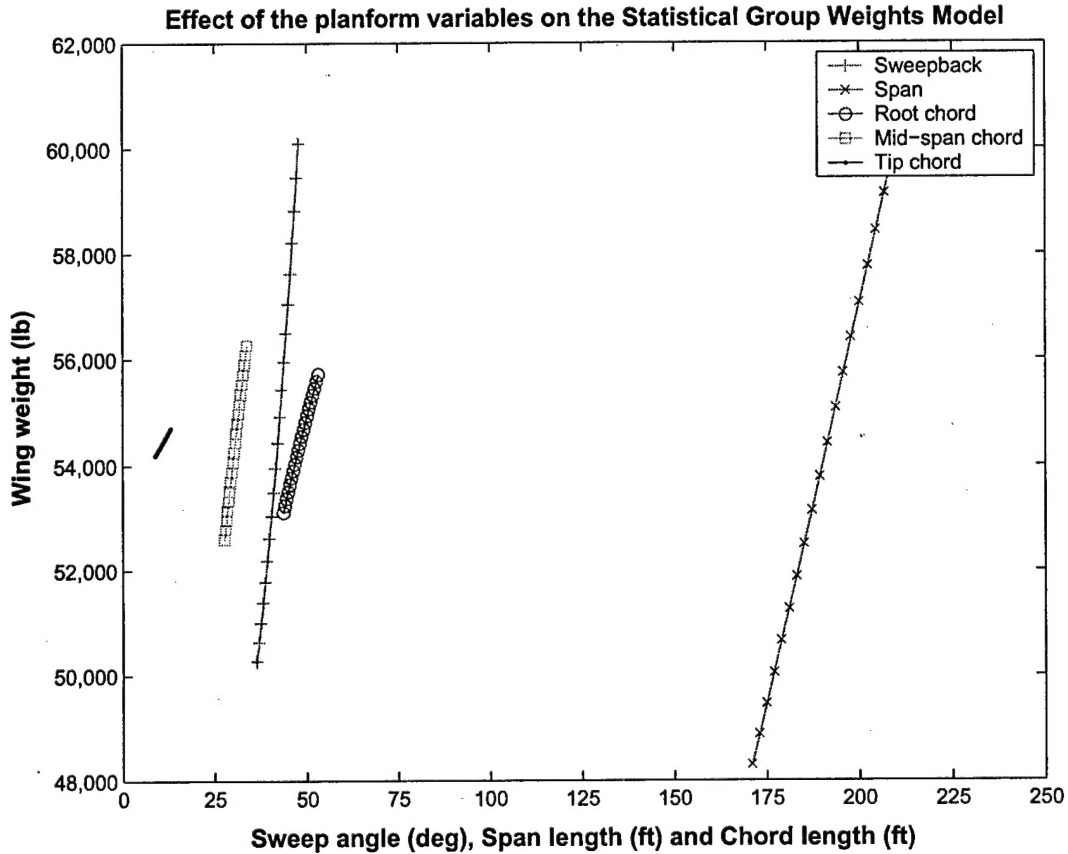

Figure 7: Effect of sweepback(Λ), span (b), root chord(c_1), mid-span chord(c_2), and tip chord(c_3) on the Statistical Group Weights Method

If c_1, c_2, or c_3 is allowed to vary, and again α_3 is chosen to be sufficiently large in the cost function (9), the optimizer would be expected to reduce the chord length with a consequent increase in shock drag.

In these ways the inclusion of a weight estimate in the cost function should prevent the optimization from leading to an unrealistic wing planform, and yield to a good overall performance.

Aerodynamic Gradient Calculation for Planform Variables

Gradient information can be computed using a variety of approaches such as the finite-difference method, the complex step method, and the automatic differentiation. Unfortunately, their computational cost is still proportional to the number of design variables in the problem. In an optimum transonic wing design, suppose one chooses mesh points on a wing surface as the design variables, which is on the order of 1000 or more; it is impractical to calculate the gradient using the methods mentioned earlier. In our planform optimization, the design variables are points on the wing surface plus the planform variables. To evaluate the aerodynamic gradient with respect to the planform variables, since the number of planform variables (five in this study) is far less than that of the surface optimization, one could calculate the gradient by the finite-difference method, the complex step method or the automatic differentiation. However, the cost for the gradient calculation will be five times higher. A more efficient approach is to follow the adjoint formulation.

Consider the aerodynamic contribution of the cost function (9)

$$\delta I = \int_{\mathcal{B}} \delta \mathcal{M} \, d\mathcal{B}_\xi + \int_{\mathcal{D}} \psi^T \delta R \, d\mathcal{D}_\xi$$

This can be split as

$$\delta I = [I_w]_I \, \delta w + \delta I_{II}$$

with

$$\delta \mathcal{M} = [\mathcal{M}_w]_I \delta w + \delta \mathcal{M}_{II}$$

where the subscripts I and II are used to distinguish between the contributions associated with variation of the flow solution δw and those associated with the metric variations δS. Thus $[\mathcal{M}_w]_I$ represents $\frac{\partial \mathcal{M}}{\partial w}$ with the metrics fixed. Note that δR is intentionally kept unsplit for programming purposes. If one chooses ψ as ψ^*, where ψ^* satisfies

$$(S_{ij} \frac{\partial f_j}{\partial w})^T \frac{\partial \psi^*}{\partial \xi_i} = 0,$$

then

$$
\begin{aligned}
\delta I(w, S) &= \delta I(S) \\
&= \int_{\mathcal{B}} \delta \mathcal{M}_{II} \, d\mathcal{B}_\xi + \int_{\mathcal{D}} \psi^{*^T} \delta R \, d\mathcal{D}_\xi \\
&\approx \sum_{\mathcal{B}} \delta \mathcal{M}_{II} \Delta \mathcal{B} + \sum_{\mathcal{D}} \psi^{*^T} \Delta \bar{R} \\
&\approx \sum_{\mathcal{B}} \delta \mathcal{M}_{II} \Delta \mathcal{B} + \sum_{\mathcal{D}} \psi^{*^T} \left(\bar{R}|_{S+\delta S} - \bar{R}|_S \right),
\end{aligned}
$$

where $\bar{R}|_S$ and $\bar{R}|_{S+\delta S}$ are volume weighted residuals calculated at the original mesh and at the mesh perturbed in the design direction.

Provided that ψ^* has already been calculated and $\bar{R}$ can be easily calculated, the gradient of the planform variables can be computed effectively by first perturbing all the mesh points along the direction of interest. For example, to calculate the gradient with respect to the sweepback, move all the points on the wing surface as if the wing were pushed backward and also move all other associated points in the computational domain to match the new location of points on the wing. Then re-calculate the residual value and subtract the previous residual value from the new value to form $\Delta \bar{R}$. Finally, to calculate the planform gradient, multiply $\Delta \bar{R}$ by the costate vector and add the contribution from the boundary terms.

This way of calculating the planform gradient exploits full benefit of knowing the value of adjoint variables ψ^* with no extra cost of flow or adjoint calculations.

Choice of Weighting Constants

The choice of α_1 and α_3 greatly affects the optimum shape. An intuitive choice of α_1 and α_3 can be made by considering the problem of maximizing range of an aircraft. The simplified range equation can be expressed

as

$$R = \frac{V}{C}\frac{L}{D}log\frac{W_1}{W_2}$$

where
C = Specific Fuel Consumption,
D = Drag,
L = Lift,
R = Range,
V = Aircraft velocity,
W_1 = Take off weight, and
W_2 = Landing weight.
If one takes

$$W_1 = W_e + W_f = \text{fixed}$$
$$W_2 = W_e$$

where
W_e = Gross weight of the airplane without fuel, then the variation of the weight can be expressed as
W_f = Fuel weight,

$$\delta W_2 = \delta W_e.$$

With fixed $\frac{V}{C}$, W_1, and L, the variation of R can be stated as

$$\delta R = \frac{V}{C}\left(\delta\left(\frac{L}{D}\right)log\frac{W_1}{W_2} + \frac{L}{D}\delta\left(log\frac{W_1}{W_2}\right)\right)$$
$$= \frac{V}{C}\left(-\frac{\delta D}{D}\frac{L}{D}log\frac{W_1}{W_2} - \frac{L}{D}\frac{\delta W_2}{W_2}\right)$$
$$= -\frac{V}{C}\frac{L}{D}log\frac{W_1}{W_2}\left(\frac{\delta D}{D} + \frac{1}{log\frac{W_1}{W_2}}\frac{\delta W_2}{W_2}\right)$$

and

$$\frac{\delta R}{R} = -\left(\frac{\delta C_D}{C_D} + \frac{1}{log\frac{W_1}{W_2}}\frac{\delta W_2}{W_2}\right)$$
$$= -\left(\frac{\delta C_D}{C_D} + \frac{1}{log\frac{C_{W_1}}{C_{W_2}}}\frac{\delta C_{W_2}}{C_{W_2}}\right).$$

If we minimize the cost function defined as

$$I = C_D + \alpha C_W,$$

where α is the weighting multiplication, then choosing

$$\alpha = \frac{C_D}{C_{W_2}log\frac{C_{W_1}}{C_{W_2}}}, \qquad (12)$$

corresponds to maximizing the range of the aircraft.

Design Cycle

The design cycle starts by first solving the flow field until at least a 4 order of magnitude drop in the residual. The flow solution is then passed to the adjoint solver. Second, the adjoint solver is run to calculate the costate vector. Iteration continues until at least a 4 order of magnitude drop in the residual. The costate vector is passed to the gradient module to evaluate the aerodynamic gradient. Then, the structural gradient is calculated and added to the aerodynamic gradient to form the overall gradient. The steepest descent method is used with a small step size to guarantee that the solution will converge to the optimum point. The design cycle is shown in Figure 8.
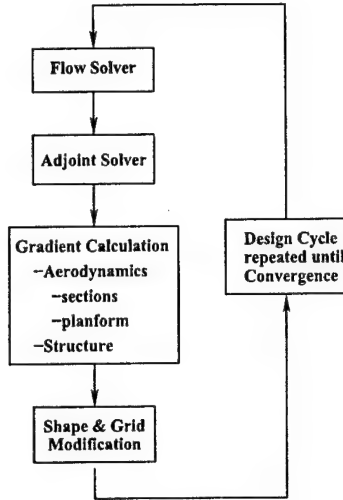
Figure 8: Design cycle

Applications to Aero-Structural Optimization

During the course of this grant, we have developed and implemented a high-fidelity aero-structural optimization framework that allows the optimization of aircraft configurations described by the full Euler or Navier-Stokes equations and a complete linear finite element model of the structure. The framework has been recently completed and uses a coupled aero-structural adjoint procedure to compute coupled sensitivities of both aerodynamic and structural cost functions to design variables that parameterize the shape of both the outer mold line and the structure itself. The accuracy of the sensitivities has been demonstrated and their use in realistic design has also been presented. In order to reduce the cost of computation of the sensitivities of the finite element stresses, Kreisselmeier-Steinhauser (K-S) functions are used to lump the constraints in the problem.

With a suitable definition of the design variables and constraints, we are seeking to solve the following aircraft design optimization problem:

$$\begin{aligned} \text{minimize} \quad & I = \alpha C_D + \beta W \\ x_A, x_S \in \mathbb{R}^n \\ \text{subject to} \quad & C_L = C_{L_T} \\ & KS \geq 0 \\ & x_S \geq x_{S_{\min}}. \end{aligned}$$

with the use of the coupled adjoint procedure to calculate the sensitivities required by the optimizer.

Aero-Structural Sensitivity Analysis

For the case of aero-structural sensitivities, we have coupled aerodynamic (R_A) and structural (R_S) governing equations, and two sets of state variables: the flow state vector, w, and the vector of structural displacements, u. In the following expressions, we split the vectors of residuals, states and adjoints into two smaller vectors corresponding to the aerodynamic and structural systems, i.e.

$$R = \begin{bmatrix} R_A \\ R_S \end{bmatrix}, \quad y = \begin{bmatrix} w \\ u \end{bmatrix}, \quad \psi = \begin{bmatrix} \psi_A \\ \psi_S \end{bmatrix}. \tag{13}$$

Figure 9 shows a diagram representing the coupling in this system. Using this new notation, the adjoint equation for an aero-structural system can be written as

$$\begin{bmatrix} \frac{\partial R_A}{\partial w} & \frac{\partial R_A}{\partial u} \\ \frac{\partial R_S}{\partial w} & \frac{\partial R_S}{\partial u} \end{bmatrix}^T \begin{bmatrix} \psi_A \\ \psi_S \end{bmatrix} = - \begin{bmatrix} \frac{\partial I}{\partial w} \\ \frac{\partial I}{\partial u} \end{bmatrix}. \tag{14}$$
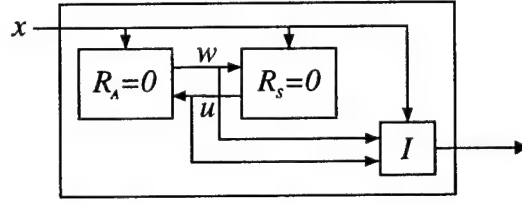
Figure 9: Schematic Representation of the Aero-Structural Governing Equations.

In addition to the diagonal terms of the matrix that appear when we solve the single discipline adjoint equations, we also have off-diagonal terms expressing the sensitivity of one discipline to the state variables of the other. The residual sensitivity matrix in this equation is identical to that of the Global Sensitivity Equations (GSE) introduced by Sobieski.

Since the factorization of the full matrix in the system of equations (14) would be extremely costly, our approach uses an iterative solver, much like the one used for the aero-structural solution, where the adjoint vectors are *lagged* and the two different sets of equations are solved separately. For the calculation of the adjoint vector of one discipline, we use the adjoint vector of the other discipline from the previous iteration, i.e., we solve

$$\left[\frac{\partial R_A}{\partial w}\right]^T \psi_A = -\frac{\partial I}{\partial w} - \left[\frac{\partial R_S}{\partial w}\right]^T \tilde{\psi}_S, \tag{15}$$

$$\left[\frac{\partial R_S}{\partial u}\right]^T \psi_S = -\frac{\partial I}{\partial u} - \left[\frac{\partial R_A}{\partial u}\right]^T \tilde{\psi}_A, \tag{16}$$

where $\tilde{\psi}_A$ and $\tilde{\psi}_S$ are the lagged aerodynamic and structural adjoint vectors. The final result given by this system, is the same as that of the original coupled-adjoint equations (14). We call this the *Lagged-Coupled Adjoint* (LCA) method for computing sensitivities of coupled systems. Note that these equations look like the single discipline adjoint equations for the aerodynamic and the structural solvers, with the addition of forcing terms in the right-hand-side that contain the off-diagonal terms of the residual sensitivity matrix. Note also that, even for more than two disciplines, this iterative solution procedure is nothing but the well-known Block-Jacobi method.

As noted previously, $\partial R_S/\partial u = K$ for a linear structural solver. Since the stiffness matrix is symmetric ($K^T = K$) the structural equations (16) are self-adjoint. Therefore, the structural solver can be used to solve for the structural adjoint vector, ψ_S, by using the *pseudo-load* vector given by the right-hand-side of equation (16).

Once both adjoint vectors have converged, we can compute the final sensitivities of the objective function by using

$$\frac{dI}{dx} = \frac{\partial I}{\partial x} + \psi_A^T \frac{\partial R_A}{\partial x} + \psi_S^T \frac{\partial R_S}{\partial x}, \tag{17}$$

which is the coupled version of the total sensitivity equation. In order to solve the aircraft optimization problem we proposed earlier on, we also need sensitivities of the structural weight with respect to the design variables. Since the aero-structural coupling does not involve the weight, these sensitivities are easily computed.

Figure 10 below shows the coupled aero-structural sensitivities of the C_D with respect to a number of aerodynamic shape variables on the upper surface of a supersonic business jet wing. The agreement of our method, in comparison with results produced with the complex-step formulation is quite good. Similar agreement is found for structural cost functions and structural design variables.
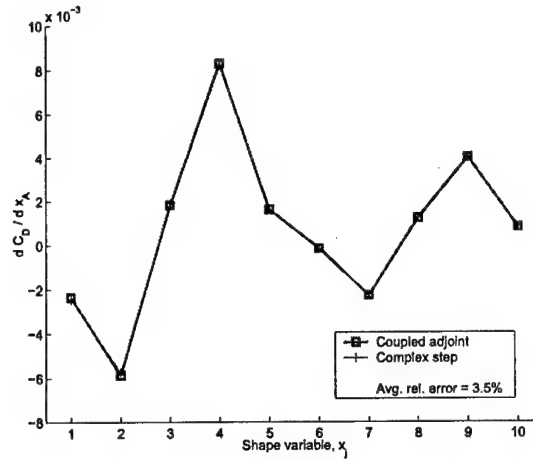
13

Figure 10: Sensitivities of the Drag Coefficient with Respect to Shape Perturbations.

Aero-Structural Design

The objective in this optimization is to solve the design problem that we previously described, i.e.,

$$\text{minimize} \quad I = \alpha C_D + \beta W$$
$$x \in \mathbb{R}^n$$
$$\text{subject to} \quad C_L = C_{L_T}$$
$$\text{KS} \geq 0$$
$$x \geq x_{\min}.$$

In our example the value of C_D corresponds to that of the cruise condition, which has a target lift coefficient of 0.1. The structural stresses, in the form of the KS function, correspond to a single maneuver condition, for which $C_{L_T} = 0.2$.

All optimization work is carried out using the nonlinear constrained optimizer NPSOL, Euler calculations are performed on a wing-body 36-block mesh that is constructed from the decomposition of a $193 \times 33 \times 49$ C-H mesh. During the process of optimization, all flow evaluations are converged to 5.3 orders of magnitude of the average density residual and the C_L constraint is satisfied within 10^{-6}.

In order to parameterize the shape of the aircraft, we have chosen sets of design variables that apply to both the wing and the fuselage. The wing shape is modified by the design optimization procedure at six defining stations uniformly distributed from the side-of-body to the tip of the wing. The shape modifications of these defining stations are linearly lofted to a zero value at the previous and next defining stations. On each defining station, the twist, the leading and trailing edge camber distributions, and five Hicks–Henne bump functions on both the upper and lower surfaces are allowed to vary. The leading and trailing edge camber modifications are not applied at the first defining station. This yields a total of 76 OML design variables on the wing. Planform modifications, which are permitted by our software, were not used in the present calculations. Planform optimization is only meaningful if additional disciplines and constraints are taken into account.

The shape of the fuselage is parameterized in such a way that its camber is allowed to vary while the total volume remains constant. This is accomplished with 9 bump functions evenly distributed in the streamwise direction starting at the 10% fuselage station. Fuselage nose and trailing edge camber functions are added to the fuselage camber distribution in a similar way to what was done with the wing sections.

The structural sizing is accomplished with 10 design variables, which correspond to the skin thicknesses of the top and bottom surfaces of the wing. Each group is formed by the plate elements located between two adjacent ribs. All structural design variables are constrained to exceed a specified minimum gauge value.

The complete configuration is therefore parameterized with a total of 97 design variables. As mentioned in an earlier section, the cost of aero-structural gradient information using our coupled-adjoint method is
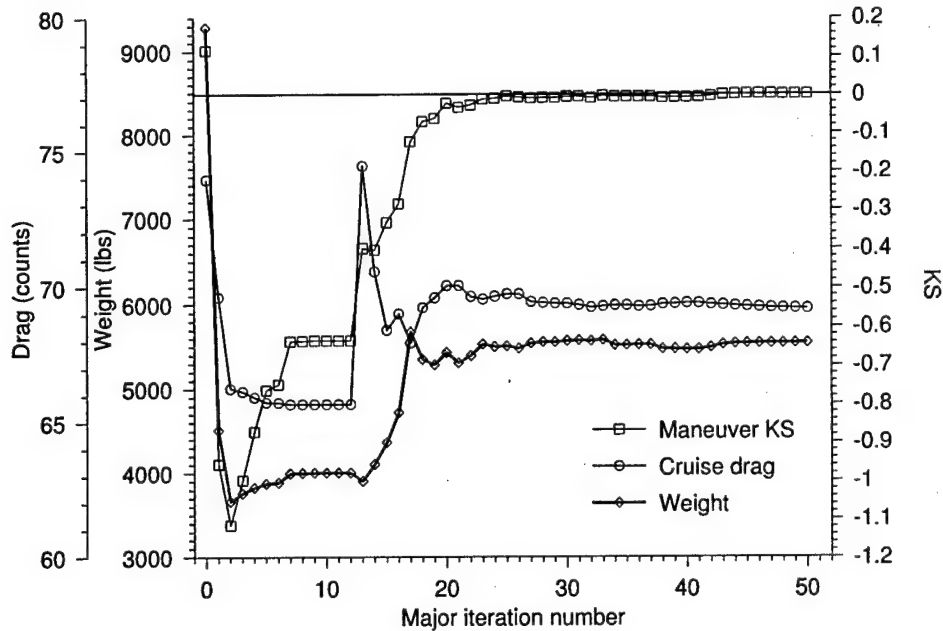
14

Figure 11: Convergence history of the aero-structural optimization.

effectively independent of the number of design variables: in more realistic full configuration test cases that we are about to tackle, 500 or more design variables will be necessary to describe the shape variations of the configuration (including nacelles, diverters, and tail surfaces) and the sizing of the structure.

The initial application of our design methodology to the aero-structural design of a supersonic business jet is simply a proof-of-concept problem meant to validate the sensitivities obtained with our method. Current work is addressing the use of multiple realistic load conditions, dynamic loads, aeroelastic constraints, and the addition of diverters, nacelles, and empennage.

In the present design case, we use $\alpha = 10^4$, $\beta = 3.226 \times 10^{-3}$. Note that the scalars that multiply the structural weight, W, and the coefficient of drag, C_D, reflect the correct trade-off between drag and weight that was previously mentioned, i.e. that one count of drag is worth 310 pounds of weight.

Figure 11 shows the evolution of this aero-structural design case for successive major design iterations. The figure shows the values of the coefficient of drag (in counts), the wing structural weight (in lbs), and the value of the KS function. Note that the structural constraints are satisfied when the KS function is positive. Because of the approximate nature of the KS function, all structural constraints may actually be satisfied for small but negative values of the KS function.

The baseline design is feasible, with a cruise drag coefficient of 74.04 counts and a structural weight of 9,285 lbs. The KS function is slightly positive indicating that all stress constraints are satisfied at the maneuver condition. In the first two design iterations, the optimizer takes large steps in the design space, resulting in a drastic reduction in both C_D and W. However, this also results in a highly infeasible design that exhibits maximum stresses that have a value of 2.1 times the yield stress of the material. After these initial large steps, the optimizer manages to decrease the norm of the constraint violation. This is accomplished by increasing the structural skin thicknesses while decreasing the airfoil thicknesses, resulting in a weight increase and a further reduction in drag. Towards major iteration 10, there is no visible progress for several iterations while the design remains infeasible. In iteration 13, a large design step results in a sudden increase in feasibility accompanied by an equally sudden increase in C_D. The optimizer has established that the best way of obtaining a feasible design is to increase the wing thickness (with the consequent increases in C_D and weight) and the structural thicknesses. From that point on, the optimizer rapidly converges to the optimum. After 43 major iterations, the KS constraint is reduced to $\mathcal{O}(10^{-4})$ and all stress constraints are satisfied. The aero-structurally optimized result has $C_D = 0.006922$ and a total wing structure weight of 5,546 lbs.

Visualizations of the baseline and optimized configurations are shown in Figures 12 and 13. Measures of
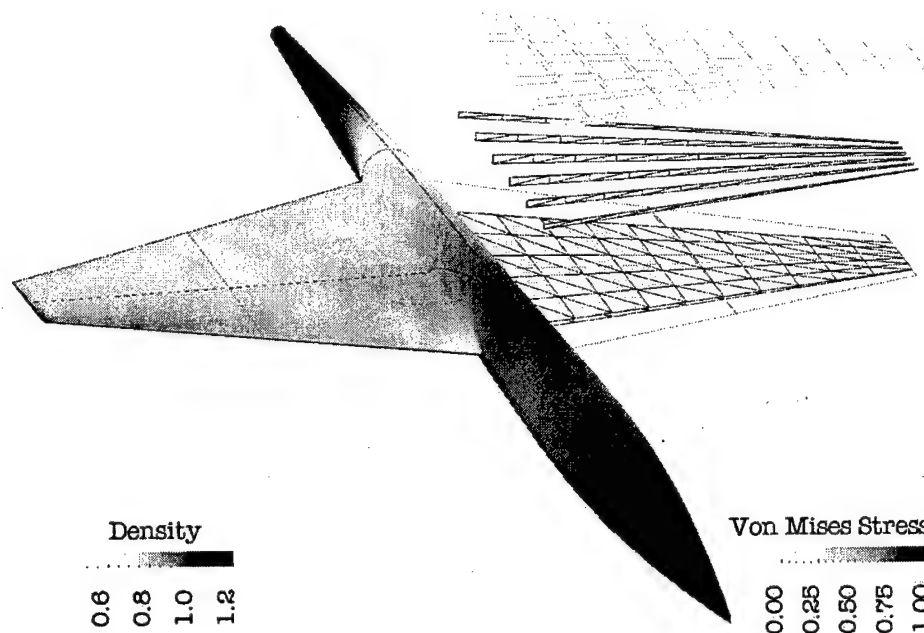
15

Figure 12: Baseline configuration for the supersonic business jet showing surface densities at the cruise condition and structural stresses at the maneuver condition. The density is normalized by the freestream value and the von Mises stresses are normalized by the material yield stress.

performance and feasibility are presented in the first section of Table 2. The left halves of Figures 12 and 13 show the surface density distributions with the corresponding structural deflections at the cruise condition for both the initial and optimized designs. The right halves show exploded views of the stress distributions on the structure (spar caps, spar shear webs, and skins, from top to bottom) at the $C_L = 0.2$ maneuver condition. From these Figures one can appreciate that not only have the surface density distributions changed substantially at the cruise point, but so have the element stresses at the maneuver condition. In fact, as expected from a design case with a single load condition, the optimized structure is exhibits stresses much closer to the yield stress, except in the outboard sections of the wing, where the minimum gauge constraints are active. It is also worth noting that about half of the improvement in the C_D of the optimized configuration results from drastic changes in the fuselage shape: both front and aft camber have been added to distribute the lift more evenly in the streamwise direction in order to reduce the total lift-dependent wave drag.

A total of 50 major design iterations including aero-structural analyses, coupled adjoint solutions, gradient computations, and line searches were performed in approximately 20 hours of wall clock time using 18 processors of an SGI Origin 3000 system (R12000, 400 MHz processors). Since these are not the fastest processors currently available we feel confident that much larger models can be optimized with overnight turnaround in the near future.

Comparison with Sequential Optimization

The usefulness of a coupled aero-structural optimization method can only be measured by comparing with the results obtained using current state-of-the-art practices. In the case of aero-structural design, the typical approach is to carry out aerodynamic shape optimization with artificial airfoil thickness constraints meant to represent the effect of the structure, followed by structural optimization with a fixed OML. It is well known that sequential optimization cannot be guaranteed to converge to the true optimum of a coupled system. In order to determine the difference between the optima achieved by fully-coupled and sequential optimizations,
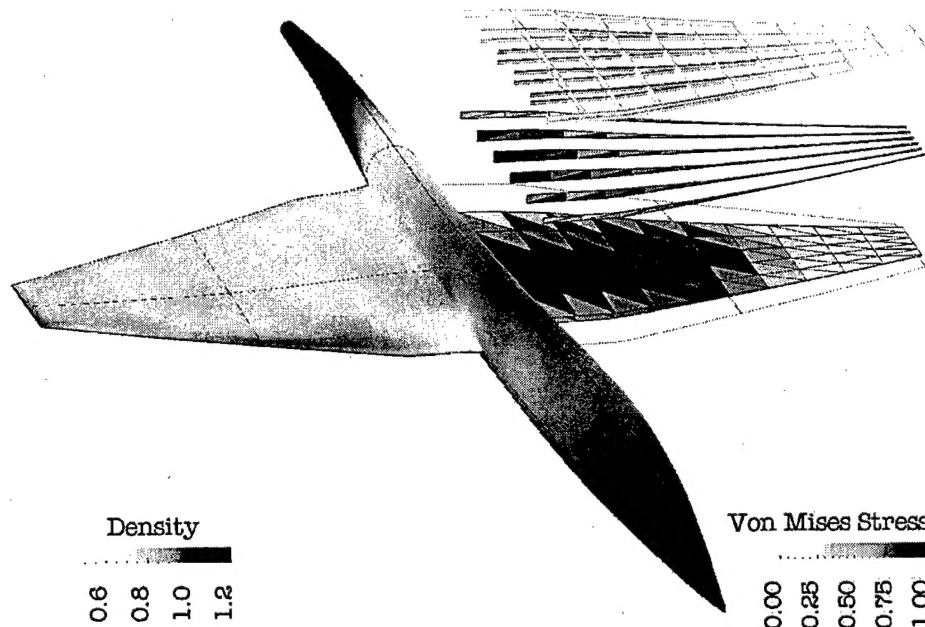
Figure 13: Optimized configuration for the supersonic business jet.

we have also carried out one cycle of sequential optimization within our analysis and design framework.

To prevent the optimizer from thinning the wing to an unreasonable degree during the aerodynamic shape optimization, 5 thickness constraints are added to each of the 6 defining stations for a total of 30 linear constraints. These constraints are such that, at the points where they are applied, the wing box is not allowed to get any thinner than the original design.

After the process of aerodynamic shape optimization is completed, the initial C_D has decreased to 0.006992, as shown in the lower portion of Table 2. After fixing the OML, structural optimization is performed using the maneuver loads for the baseline configuration at $C_L = 0.2$. The structural optimization process reduces the weight of the wing structure to 6,567 lbs.

We can now compare the results of the fully coupled optimization in the previous section and the outcome of the process of sequential optimization. The differences are clear: the coupled aero-structural optimization was able to achieve a design with a range of 7,361 nm, which is 224 nm higher than that obtained from the sequential optimization.

Finally, note that since sequential optimization neglects the aero-structural coupling in the computation of maneuver loads, there is no guarantee that the resulting design is feasible. In fact, the aero-structural analysis shows that the value of the KS function is slightly negative.

Personnel Supported

During the operational period for this grant, funds have been used to support the time of Profs. Antony Jameson and Juan J. Alonso and both Mr. Siva Kumaran and Mr. Kasidit Leoviriyakit (Ph.D. Candidates in the Department of Aeronautics & Astronautics).

	C_D (counts)	KS	$\sigma_{\max}/\sigma_y$	ZFW (lbs)	Range (nm)
Baseline	73.95	1.15×10^{-1}	0.87	47,500	6,420
Integrated optimization	69.22	-2.68×10^{-4}	0.98	43,761	7,361
Sequential optimization					
Aerodynamic optimization					
Baseline	74.04				
Optimized	69.92				
Structural optimization					
Baseline		1.02×10^{-1}	0.89	47,500	
Optimized		1.45×10^{-8}	0.98	44,782	
Aero-structural analysis	69.92	-9.01×10^{-3}	0.99		7,137

Table 2: Comparison between the integrated and sequential approaches to aero-structural optimization.

Honors/Awards

Docteur Honoris Causa. University of Paris. December 2000. AJ

Docteur Honoris Causa. Uppsala University. January 2002. AJ

Charles Lee Powell Fellowship. September 2001. JJA

Invited Lecture. "Status of CFD for Supersonic Transports", NRC Committee on Commercial Supersonic Technology. January 2001. AJ

Invited Lecture. "CFD and Optimum Aerodynamic Design", MIT Singapore Alliance. March 2001. AJ

Invited Lecture. "Design in the Era of Ultra High Speed Computers", Symposium on New Directions in Mechanical and Aerospace Engineering, Princeton University. April 2001. AJ

Invited Lecture. "Aerodynamic Shape Optimization", California Institute of Technology. May 2001. AJ

Invited Lecture. "Fast Multigrid Solutions of the Euler Equations of Gas Dynamics", ICASE, NASA Langley. June 2001. AJ

Invited Lecture. "Aero-structural Sensitivity Analysis", Sandia National Laboratories. April 2001. JJA

Invited Lecture. "Design of Low-Boom Supersonic Aircraft", UC Irvine. May 2001. JJA

Invited Lecture. "Analytic and Semi-Analytic Methods for Sensitivity Analysis of Multidisciplinary Systems", Lawrence Livermore National Laboratories. August 2001. JJA

Session Chairman. AIAA Aerospace Sciences Meeting & Exhibit, Reno, NV, January 2002. JJA & AJ
    Both Profs. Jameson and Alonso have presented work related to this grant at a number of additional venues that are not listed here but that can be seen in the list of publications that follows.

Publications

S. Nadarajah, A. Jameson, and J. J. Alonso An Adjoint Method for the Calculation of Non-Collocated Sensitivities in Supersonic Flow. First MIT Conference on Computational Fluid Dynamics, Cambridge, MA, June 2001.

S. Nadarajah and A. Jameson Studies of the Continuous and Discrete Adjoint Approaches to Viscous Automatic Aerodynamic Shape Optimization AIAA 15th Computational Fluid Dynamics Conference, AIAA-2001-2530, Anaheim, CA, June 2001.

A. Jameson and D. Caughey How Many Steps are Required to Solve the Euler Equations of Steady Compressible Flow: In Search of a Fast Solution Algorithm. AIAA 15th Computational Fluid Dynamics Conference,

AIAA-2001-2655, Anaheim, CA, June 2001.

A. Jameson and J. Vassberg Computational Fluid Dynamics (CFD) for Aerodynamic Design: Its Current and Future Impact. AIAA 39th Aerospace Sciences Meeting and Exhibit,AIAA-2001-0538, Reno, NV, January 8-11, 2001.

A. Jameson A Perspective on Computational Algorithms for Aerodynamic Shape Analysis Progress in Aerospace Sciences, Elsevier, 2001.

J. R. R. A. Martins, J. J. Alonso, and J. Reuther Aero-Structural Wing Design Optimization Using High-Fidelity Sensitivity Analysis CEAS Conference on Multidisciplinary Aircraft Design and Optimization, Cologne, Germany, June 25-26, 2001.

S. Nadarajah, A. Jameson, and J. J. Alonso An Adjoint Method for the Calculation of Remote Sensitivities in Supersonic Flow 40th AIAA Aerospace Sciences Meeting & Exhibit, AIAA Paper 2002-0261, Reno, NV, January 2002.

A. Jameson Optimum Transonic Wing Design Using Control Theory. Symposium Transsonicum IV, International Union of Theoretical and Applied Mechanics, September 2-6, 2002, DLR Gottingen, Germany.

S. K. Nadarajah, S. Kim, A. Jameson and J. J. Alonso Sonic Boom Reduction Using an Adjoint Method for Supersonic Transport Aircraft Configuration. Symposium Transsonicum IV, International Union of Theoretical and Applied Mechanics, September 2-6, 2002, DLR Gottingen, Germany.

J. R. R. A. Martins, J. J. Alonso, and J. Reuther High-Fidelity Aero-Structural Design Optimization of a Supersonic Business Jet. 43rd AIAA Structures, Structural Dynamics and Materials Conference, AIAA Paper 2002-1483, Denver, CO, April 2002.

S. K. Nadarajah, A. Jameson and J. J. Alonso Sonic Boom Reduction using an Adjoint Method for Wing-Body Configurations in Supersonic Flow 9th AIAA/ISSMO Symposium on Multidisciplinary Analysis and Optimization Conference, AIAA-2002-5547, September 4-6, 2002, Atlanta, GA.

S. K. Nadarajah and A. Jameson Optimal Control of Unsteady Flows using a Time Accurate Method. 9th AIAA/ISSMO Symposium on Multidisciplinary Analysis and Optimization Conference, AIAA-2002-5436, September 4-6, 2002, Atlanta, GA.

K. Leoviriyakit and A. Jameson Aerodynamic Shape Optimization of Wings including Planform Variations 41st AIAA Aerospace Sciences Meeting & Exhibit, AIAA Paper 2003-0210, Reno, NV, January 6-9, 2003.

A. Jameson and S. Kim Reduction of the Adjoint Gradient Formula in the Continous Limit 41st AIAA Aerospace Sciences Meeting & Exhibit, AIAA Paper 2003-0040, Reno, NV, January 6-9, 2003.

A. Jameson Aerodynamic Shape Optimization Using the Adjoint Method Lecture Series at the Von Karman Institute, Febuary 6, 2003, Brussels, Belgium.

A. Kim, K. Leoviriyakit and A. Jameson Aerodynamic shape and planform optimization of wings using a viscous reduced adjoint gradient formula 2nd M.I.T. Conference on Computational Fluid and Solid Mechanics, Cambridge, MA, June 17-20, 2003.

S. Nadarajah, M. McMullen and A. Jameson Optimal Control of Unsteady Flows Using Time Accuraate and Non-Linear Frequency Domain Methods 33rd AIAA Fluid Dynamics Conference and Exhibit, AIAA Paper AIAA-2003-3875, Orlando, FL, June 23-26, 2003.

A. Jameson Aerodynamic Design and Optimization 16th AIAA Computational Fluid Dynamics Conference, AIAA Paper AIAA-2003-3438, Orlando, FL, June 23-26, 2003.

J. J. Alonso, J. R. R. A. Martins, J. J. Reuther, R. Haimes and C. A. Crawford High-Fidelity Aero-Structural Design Using a Parametric CAD-Based Model 16th AIAA Computational Fluid Dynamics Conference, AIAA Paper AIAA-2003-3429, Orlando, FL, June 23-26, 2003.

K. Leoviriyakit, S. Kim and A. Jameson Viscous Aerodynamic Shape Optimization of Wings Including Planform Variables 21st AIAA Applied Aerodynamics Conference, AIAA Paper AIAA-2003-3531, Orlando, FL, June 23-26, 2003.

A. Jameson Time Integration Methods in Computational Aerodynamics 2003 AFOSR Work Shop on Advances and Challenges in Time-Integration of PDEs, Providence, RI, August 18, 2003.

A. Jameson The Role of CFD in Preliminary Aerospace Design 4th ASME-JSME Joint Fluids Engineering Conference, ASME Paper FEDSM2003-45812, Honolulu, Hawaii, July 6-11, 2003.